International Journal of Impact Engineering 95 (2016) 141–153

Contents lists available at ScienceDirect

International Journal of Impact Engineering

journal homepage: www.elsevier.com/locate/ijimpeng

# The elastic-plastic dynamic response of stiffened plates under confined blast load

Cheng Zheng [a,b], Xiang-shao Kong [a,b,*], Wei-guo Wu [a,b], Fang Liu [b]

[a] Ministry of Education, Key Laboratory of High Performance Ship Technology, Wuhan University of Technology, Wuhan 430063, China
[b] Departments of Naval Architecture, Ocean and Structural Engineering, School of Transportation, Wuhan University of Technology, Wuhan 430063, China

ARTICLE INFO

*Article history:*
Received 7 October 2015
Received in revised form 17 March 2016
Accepted 10 May 2016
Available online 13 May 2016

*Keywords:*
Confined blast load
Square stiffened plates
Yield line pattern
Elastic-plastic effect
Large deflection

ABSTRACT

The large-deflection behavior of the clamped stiffened plates subjected to confined blast load is investigated through experimental tests, theoretical calculation and numerical simulation in this paper. The blast load in confined space lasts longer and has more complex form compared to the shock waves from an open space explosion. The influence of elastic-plastic effect on the dynamic response of blast loaded plate should be taken into account in theoretical prediction of permanent displacement. Besides, evident yield lines, which could change the deformed shape of the plates, can be always found around the clamped edges and the diagonals of plates. The global deformation of a plate cannot be represented by a simple shape function of a smooth surface. In this paper, a series of experimental tests of square stiffened plates under confined blast load was conducted. Based on experimental observation and assumed-modes, an elastic-plastic analytical model for blast loaded stiffened plates is presented, in which the effects of yield line pattern and elastic-plastic deformation are considered. The Lagrange motion equation that contains the total strain energy, potential energy and kinetic energy of stiffened plates and blast load system is established and solved. Numerical simulations are performed to investigate the influence of strain rate effect of material and boundary conditions on the dynamic responses of stiffened plates. By comparing the numerical results, the rationality of hypothetic conditions employed in analytical model is verified. The classical rigid-plastic and elastic-plastic methods were also used to calculate the dynamic response and permanent displacements of test specimens. The comparison results showed that the theoretical calculation model presented in this paper is feasible and of high precision and practicability.



## 1. Introduction

The stiffened plate is the most fundamental structure and widely used in marine industry such as ship hull and offshore topside structures. These structures are occasionally subjected to blast hazard such as gas explosion, free air blast or confined blast load during combat environment or terrorist attack. The blast hazard in these structures will lead to total collapse of facilities and loss of life. It is of great importance to predict dynamic responses of blast loaded plates in design phase to ensure the safety of structures or reduce the level of damage. Explosively driven dynamic response of ductile metals is a very complex process which involves events such as plastic flow at relative high strain rates, large elastic-plastic deformation and tear failure of plates. Researches in this filed are focused on the two most important aspects: determination of blast load from explosions and prediction of dynamic responses of stiffened plates using experimental, numerical and theoretical approaches [1–7].

The rigid, perfectly plastic method used to estimate the residual deformation of metal plate was firstly developed by Jones [8–10]. In general, yield lines formed in plates were always taken into account in rigid-plastic analytical models for blast loaded plates [9–13]. The rectangular plate was modeled with rigid segments interconnected by yield lines, which yielded a roof-shaped displacement in most rigid-plastic analytical models. This method provided relatively accurate results when the ratio of initial kinetic energy to maximum possible elastic strain energy was larger than about 10 and the load pulse duration was sufficiently short with respect to the fundamental natural period of elastic vibration. Based on rigid-plastic membrane theory and the concept of the instantaneous mode approximation technique, a theoretical model was present by Nurick and Martin [14,15] to predict the transverse displacements of thin circular, square and rectangular plates subjected to transverse impulsive loading, and the results from the model agreed well with the experimental data in the range where the permanent displacement was up to 12 times the thickness of the plate. Besides, a lot of interesting research works related to the dynamic responses of plates were presented, and some simplified theoretical models were also proposed and validated by experimental or numerical results [16–22].

* Corresponding author. Ministry of Education, Key Laboratory of High Performance Ship Technology, Wuhan University of Technology, Wuhan 430063, China. Tel.: 0086-13476068165; Fax: 0086-27-86551193.
*E-mail address:* kongxs@whut.edu.cn (X. Kong).

http://dx.doi.org/10.1016/j.ijimpeng.2016.05.008
0734-743X/

**Nomenclature**

| | |
|---|---|
| $w$ | transverse displacement of plate |
| $w_1$ | transverse displacement of surrounding parts |
| $w_2$ | transverse displacement of central part |
| $Z_1$, $Z_2$ | generalized transverse displacements |
| $\dot{Z}_1$, $\dot{Z}_2$ | generalized transverse velocities |
| $\ddot{Z}_1$, $\ddot{Z}_2$ | generalized transverse accelerations |
| $\varepsilon_x$, $\varepsilon_y$ | in-plane strains in x and y direction |
| $\gamma_{xy}$ | in-plane shear strain in x–y plane |
| $u$, $v$ | horizontal and longitudinal displacements |
| $\varepsilon_0$ | in-plane elastic limit strain |
| $\gamma_0$ | in-plane elastic limit shear strain |
| $U_{\text{c-b}}$ | bending strain energy of central part of plate |
| $U_{\text{c-me}}$ | elastic membrane strain energy of central part of plate |
| $U_{\text{c-mp}}$ | plastic membrane strain energy of central part of plate |
| $U_{\text{s-me}}$ | elastic membrane strain energy of surrounding parts of plate |
| $U_{\text{s-mp}}$ | plastic membrane strain energy of surrounding parts of plate |
| $U_{\text{st}}$ | strain energy of stiffeners |
| $U_{\text{l}}$ | strain energy of plastic hinges in the plate |
| $\varepsilon$ | in-plane strain of surrounding parts of plate |
| $L$ | length of one-quarter symmetry model |
| $l$ | projected length of yield lines in x direction |
| $\sigma_0$ | static yield stress |
| $\sigma_{\text{d}}$ | dynamic yield stress |
| $\tau_0$ | elastic limit of shear stress |
| $\delta$ | plate thickness |
| $\theta$ | the rotation angle of plastic hinge along clamped edges |
| $\theta_1$ | the rotation angle of plastic hinge along connecting lines of central and surrounding part |
| $\theta_2$ | the rotation angle of oblique plastic hinge along the diagonals of plate |
| $M_{\text{p}}$ | the plastic bending strain energy of plate with unit width |
| $p(t)$ | magnitude of pressure loading at time $t$ |
| $P$ | magnitude of equivalent rectangular pressure load |
| $\tau_d$ | duration of simplified blast load |
| $U$ | total strain energy |
| $V$ | total potential energy |
| $T$ | kinetic energy |
| $M_{\text{s}}$ | the moment of the plastic hinge in the stiffener |
| $P_{\text{E}}$ | loss of potential energy of load |
| $\rho$ | density of material |
| $\dot{w}$ | transverse velocity |
| $w_{\text{s}}$ | transverse displacement of stiffener |
| $x_{\text{s}}$ | the X position of the stiffener in x–y plane |
| $\theta_{\text{s}}$ | the rotation angle of the plastic hinge in the stiffener |
| $E$ | Young's modulus of materials |
| $A$ | cross-sectional area of the stiffener |
| $b$ | thickness of the stiffener |
| $h$ | height of the stiffener |
| $I$ | 2nd moment of area of stiffener |

While a rapidly decayed blast load is applied instantaneously and the intensity is several times larger than the static collapse load of structure, large deformation occurs within a very short time of the order of microseconds. The rigid-plastic method is appropriate for the rapid assessment of dynamic response of blast loaded structures. However, when an explosion occurs in a confined space, the characteristics of blast load are different from those in open circumstance. A quasi-static pressure load with a long duration will be generated after initial and reflected shock waves due to limitation of structures [5]. Symonds and Frye [23] demonstrated that when the pulse duration was relatively long or the structure was relatively stiff, the rigid-plastic solution was non-conservative compared with the elastic-plastic solution. A series of tests was conducted by Schleyer et al. [7] to study the dynamic large-deflection of mild steel plates subjected to uniform pulse pressure loads with a longer total pulse duration. Multi-element elastic-plastic models of stiffened plates were developed by Schleyer et al. [6,7,24–28] in which the bi-axial behavior of the plate was represented by one-dimensional finite strips. The in-plane restraint of the plate was approximated using non-linear translation springs. Turvey and Salehi [29] proposed an elastic-plastic theory to analyze the large deformation behavior of circular stiffened plates, and the corresponding discrete solution was also presented in their publication.

In previous research, the assumed-mode analysis was based on simple structural models in which stiffened plates were assumed to deform in a prescribed form. The deformation shape function of a square plate was always simplified as a cosine or sine function [6,7,27,28]. The work of Schleyer and co-workers [6,7] used non-linear rotational spring elements to model the onset of a plastic hinge, but did not incorporate the yield line pattern or the potential transient movement of the plastic hinge. However, the experimental observations had revealed that evident yield lines could be found around the sides and the diagonals of plates under intense dynamic loads [7]. Yield lines could greatly change the deformed shape of the plates during the dynamic process. Therefore, the global deformation of a plate cannot be represented by a simple shape function approximately.

In this paper, experimental tests of stiffened plates under confined blast load were firstly conducted in Section 2. In Section 3, an elastic-plastic analytical approach for blast loaded stiffened plates is presented, which considers the influences of membrane force, elastic deformation and yield line pattern in deformed plates. In analytical model, the deformed stiffened plate is divided into two different parts composed of the central region with smooth surface and the surrounding plastic stretch zone, and corresponding shape functions are given. Based on energy conservation and Lagrange's equation, the dynamic response of the stiffened plate is derived by theoretical calculation. In Section 4, numerical simulations are performed to investigate the influence of strain rate effect of material. The classical rigid-plastic and elastic-plastic methods were also employed to obtain the permanent displacements of test specimens. The conclusions and discussions are finally presented in Section 5.

## 2. Experimental tests

In this paper, a series of experimental tests of clamped stiffened plates subjected to confined blast load was carried out, and the permanent displacements of test plates were obtained.

### 2.1. Test facility and specimens

The experimental device was designed to produce confined blast load acting on the stiffened plates. The device is actually a structural chamber made from high strength steel as shown in Fig. 1. The construction and dimension of the device are shown schematically in Fig. 2. The length of the device is 1800 mm, and both the width


(a) (b)

**Fig. 1.** Test facility of stiffened plates under confined blast load.

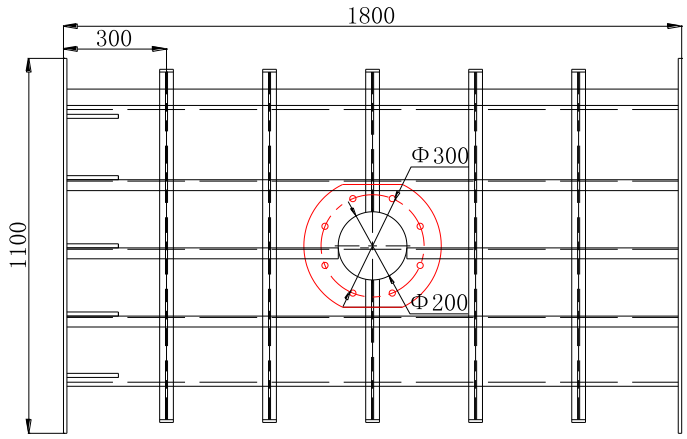


(a) Front view (dimension in mm)

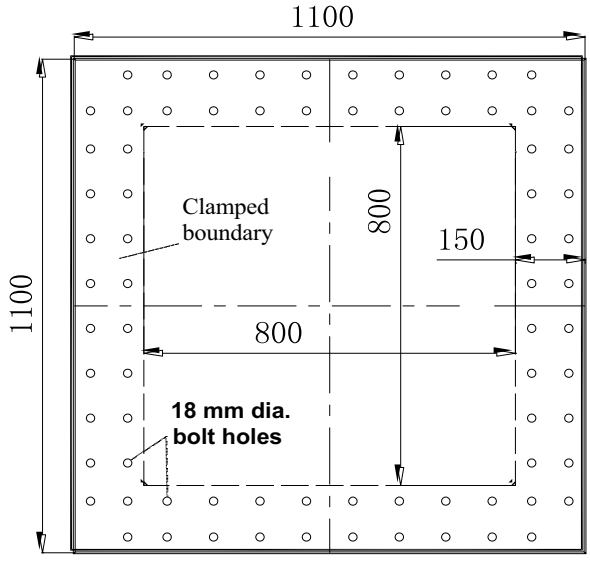


(b) Side view (dimension in mm)

**Fig. 2.** Dimension of the experimental setup. (a) Front view (dimension in mm). (b) Side view (dimension in mm).

and the height are 1100 mm. The chamber was designed to be strong enough to minimize the deformation of walls under confined blast load. A venting hole is located at the center of the front wall, as shown in Fig. 3. The area of venting hole can be changed through installation of different hollow flange plates to alter the blast load acting on test specimens. The test specimens were fixed upon the support plates at both ends of device by 36 M16 bolts. After the test plates were clamped to both ends, the TNT charge hung in the middle of test rig was initiated to generate blast load, as shown in Fig. 4.

The tests involved 10 square stiffened plates made from the same material. All plates used in the experiment were one-way stiffened with two or three flats, as shown in Fig. 1. The stiffened plates were clamped to both ends of the test rig with bolts and support plates. The test specimens of stiffened plates with the size of 1100 mm × 1100 mm were made from Q235 low carbon steel with different thicknesses. The effective loading area of the test stiffened plates was 800 mm × 800 mm when clamped to ends of the device. The clamping frame provided rotational and translational restraints through the support plates located against the test plates by bolts. According to the assembly requirements of the clamp frame and test plates, the diameters of bolt holes in the test plates and clamp frame are 2 mm larger than those of bolts. The geometrical size of test stiffened plates is shown in Fig. 5. The stiffened plates were manufactured by welding steel flats (800 mm long) to the plate

**Fig. 3.** Adjustable venting hole in the front wall.

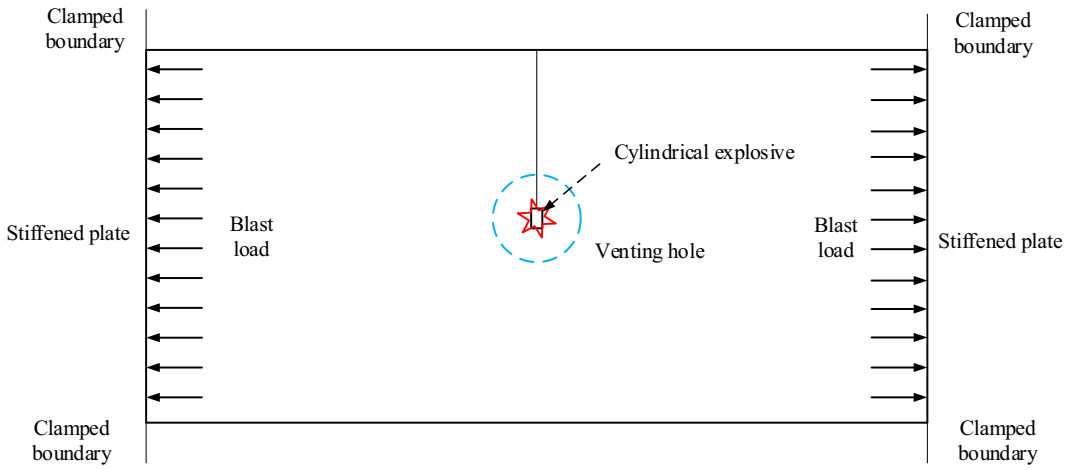


**Fig. 4.** Schematic diagram of the test rig.

using the carbon dioxide welding method. In order to minimize the distortion of the plate due to the heat generated in the welding process, the stitch welding technique was adopted in the manufacturing of the stiffened plates. The performance of the stitch welds on blast loaded plates at large deformations has been experimentally verified by Kong et al. [5].

### 2.2. Test results

Ten square stiffened plates were tested with different thicknesses and load conditions. Before dynamic tests, the ultrasonic thickness gauge was used for accurate measurement of thicknesses of plates and stiffeners. Ten cases are considered in the paper, and the corresponding geometry of test stiffened plates and load conditions including the mass of TNT and the area of venting hole are listed in Table 1. After the tests, the three-dimensional laser scanner was used to measure the permanent deformation of blast loaded plates.

Under confined blast load, all the test stiffened plates had experienced large deflection, as shown in Fig. 6. Besides, evident yield lines around the clamped boundary and along the diagonals of test specimens can be found. Yield lines greatly change the deformed shape of the plates during the dynamic response process. The deformed plate exhibits distinctive diagonal yield lines and an abrupt change in curvature across the plate, as shown in Fig. 6. The transverse displacement of different cross sections of deformed plate in case 5 is shown in Fig. 7 as an example. The measured permanent displacements at center of test plates range from 6 to 22 times the thickness of plate. In general, it is necessary to take the membrane force into consideration in analytical models when deflections are of the order of one-half the plate thickness or more. The permanent displacements at center of stiffened plates are given in Table 2. The displacement of the cross section close to clamped edges appears a flat part due to the influence of yield line pattern. It is evident that the global deformation of a plate cannot be represented by a simple shape function of a smooth surface approximately. The plate and stiffeners deformed compatibly without evident local deformation in the experiments. It seems that stiffeners on the plate have insignificant influence on the deformation shape of stiffened plates in the dynamic tests, which could be due to the weakness in bending strength and free boundary constraints at both ends of the stiffeners. Besides, the failure of the stitching welds between stiffeners and plates had not been found during the dynamic test.

**Table 1**
Dimensions of stiffened plates and load conditions.

| Plate ref. | Plate thickness $\delta$ (mm) | Number of ribs | Length of stiffeners (mm) | Thickness of stiffeners $b$ (mm) | Height of stiffeners $h$ (mm) | Radius of venting hole (mm) | Mass of TNT (g) |
|---|---|---|---|---|---|---|---|
| 1 | 1.6 | 2 | 800 | 1.6 | 20 | 50 | 55 |
| 2 | 1.6 | 2 | 800 | 1.6 | 25 | 50 | 55 |
| 3 | 1.6 | 2 | 800 | 2.3 | 25 | 50 | 55 |
| 4 | 2.3 | 2 | 800 | 2.3 | 30 | 50 | 55 |
| 5 | 2.3 | 3 | 800 | 2.3 | 30 | 50 | 55 |
| 6 | 3.7 | 2 | 800 | 2.7 | 30 | 75 | 110 |
| 7 | 3.7 | 3 | 800 | 2.7 | 30 | 75 | 110 |
| 8 | 3.7 | 3 | 800 | 2.7 | 40 | 75 | 110 |
| 9 | 4.8 | 2 | 800 | 3.7 | 30 | 100 | 200 |
| 10 | 4.8 | 2 | 800 | 4.8 | 30 | 100 | 200 |

**Table 2**
Permanent displacements of test stiffened plates.

| Plate ref. | Residual deformation (mm) | Plate ref. | Residual deformation (mm) |
|---|---|---|---|
| 1 | 35.876 | 6 | 25.919 |
| 2 | 35.374 | 7 | 24.058 |
| 3 | 33.607 | 8 | 22.243 |
| 4 | 24.926 | 9 | 32.408 |
| 5 | 23.052 | 10 | 31.511 |

## 3. Analytical methods

### 3.1. Deformation mode of blast loaded stiffened plates

The permanent displacement of stiffened plates under blast loads is generally greater than their thicknesses [7]. From the observation of experimental tests in Section 2, evident yield lines around the clamped edges and the diagonals of specimens will greatly change the deformation shape of the plates. The deformation mode of blast loaded square stiffened plate with clamped supports is shown in Fig. 8. Besides, due to the large-deflection behavior of stiffened plates under explosion, the in-plane stretching caused by the deflection should also be taken into account. Based on experimental observation, an elastic-plastic analytical model of the blast loaded plates considering the effect of the yield line and in-plane strain is established, as shown in Fig. 9. In this model, the deformed stiffened plate was divided into two parts, the central region (central part) with smooth surface and the surrounding plastic stretching zone (surrounding part). Yield lines along the clamped edges,

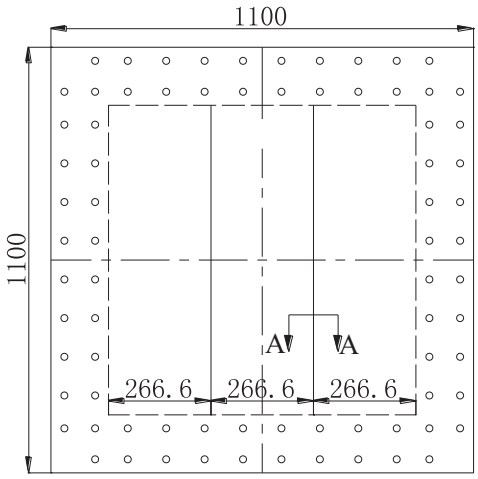


(a) Stiffened plates with two ribs (dimension in mm)

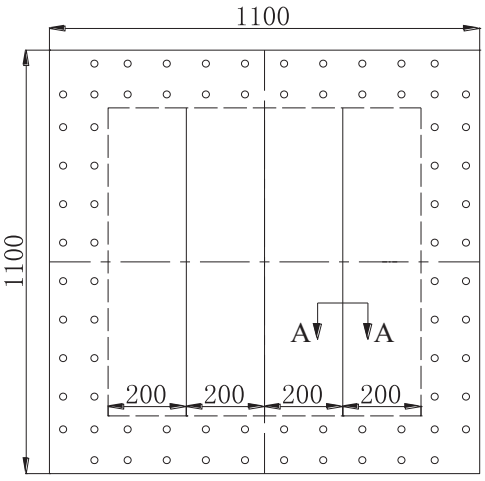


(b) Stiffened plates with three ribs (dimension in mm)

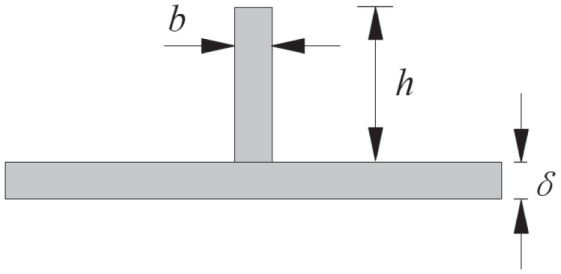


(c) Section A-A

**Fig. 5.** Geometrical size of test stiffened plates. (a) Stiffened plates with two ribs (dimension in mm). (b) Stiffened plates with three ribs (dimension in mm).

diagonal lines and connecting lines between central and surrounding parts are also considered. In the present study, it is assumed that deformation histories of plate and stiffeners are compatible during the dynamic process. As observed in experiments, the plate and stiffeners deformed together without evident local deformation. Thus, the influence of stiffeners on the deformation profile of the plate is not considered in the theoretical model. In view of symmetry of square plates, a quarter of the plate is selected in the

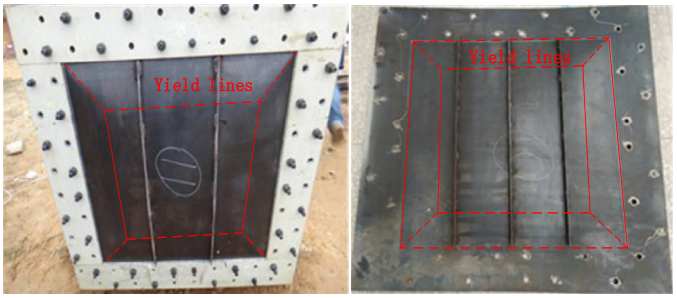


**Fig. 6.** Deformation of test stiffened plate under confined blast load.

analytical models. Based on assumed modes, the global deformation of the stiffened plate is expressed as

$$w = \begin{cases} w_1 & \text{for surrounding part} \\ Z_1 + w_2 & \text{for central part} \end{cases} \tag{1}$$

where $w_1$, $w_2$ represent transverse displacements of surrounding parts and central part, respectively. $Z_1$ is the generalized transverse displacement. The transverse displacement is the sum of $Z_1$ and $w_2$, as shown in Fig. 9.

The displacement of surrounding parts of stiffened plates is represented by:

$$w_1 = \begin{cases} \dfrac{L-x}{L-l} \cdot Z_1 & l \le x \le L;\quad 0 \le y \le x \\ \dfrac{L-y}{L-l} \cdot Z_1 & l \le y \le L;\quad 0 \le x \le y \end{cases} \tag{2}$$

The displacement of central part of stiffened plates is represented by

$$w_2 = Z_2 \cos\frac{\pi x}{2l} \cos\frac{\pi y}{2l} \quad 0 \le x, \quad y \le l \tag{3}$$

where $Z_2$ is the maximum displacement of central part based on transverse displacement $Z_1$ of surrounding part.

### 3.2. Strain energy of central part of plate

While the deflection of plate is considerably larger than its thickness, terms of third order and third order above in the Taylor expansion of strain could be neglected in the analysis for simplicity. The strain in $x$ direction is given by:

$$\varepsilon_x = \frac{\partial u}{\partial x} + \frac{1}{2}\left(\frac{\partial w_2}{\partial x}\right)^2 \tag{4}$$

Similarly, the strain in $y$ direction is given by:

$$\varepsilon_y = \frac{\partial v}{\partial y} + \frac{1}{2}\left(\frac{\partial w_2}{\partial y}\right)^2 \tag{5}$$

According to the definition of shear strain, disregarding the terms of third order and third order above, the shear strain is given by:

$$\gamma_{xy} = \frac{\partial u}{\partial y} + \frac{\partial v}{\partial x} + \frac{\partial w_2}{\partial x}\frac{\partial w_2}{\partial y} \tag{6}$$

The total potential energy of the deformed stiffened plate system mainly includes the bending strain energy of the plate in central part $U_{c\text{-}b}$, elastic-plastic membrane strain energy of the plate in central part $U_{c\text{-}m}$, the total strain energy of stiffeners in central part $U_{st}$, the elastic-plastic membrane strain energy of the plate in

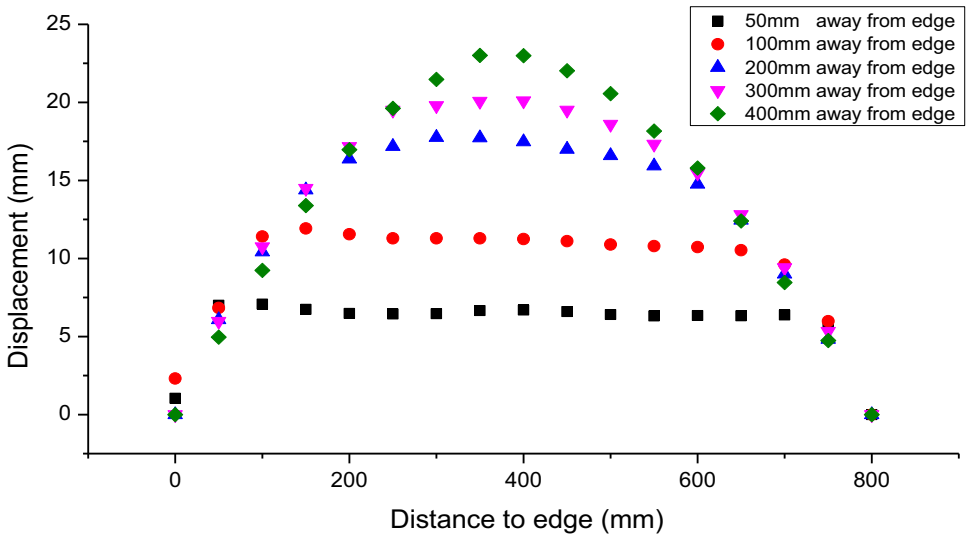


**Fig. 7.** Transverse displacements in different cross section of deformed plate with yield lines in Case 5.

surrounding parts $U_{s\text{-}m}$, the plastic strain energy of plastic hinges $U_l$ and the potential energy loss $P_E$ due to the blast load.

The bending strain energy of the plate in central part is given by

$$U_{c\text{-}b}=\frac{E\delta^3}{24(1-\upsilon^2)}\int_0^l\int_0^l\left[\left(\frac{\partial^2 w_2}{\partial x^2}\right)^2+\left(\frac{\partial^2 w_2}{\partial y^2}\right)^2+2\upsilon\frac{\partial^2 w_2}{\partial x^2}\frac{\partial^2 w_2}{\partial y^2}+2(1-\upsilon)\left(\frac{\partial^2 w_2}{\partial x\partial y}\right)^2\right]dxdy \tag{7}$$

where $\delta$ is the thickness of plate; $\upsilon$ is the Poisson's ratio of material.

The elastic membrane strain energy of the plate is given by:

$$U_{c\text{-}me}=\frac{E\delta}{2(1-\upsilon^2)}\int_0^l\int_0^l\left[\varepsilon_x^2+\varepsilon_y^2+2\upsilon\varepsilon_x\varepsilon_y+\frac{1}{2}(1-\upsilon)\gamma_{xy}^2\right]dxdy \tag{8}$$

The Eq. (8) can be only used for calculating the elastic membrane strain energy of the plate. After the yielding occurs, the plastic strain energy of the plate should be determined. In this paper, the elastic perfectly-plastic material, as shown in Fig. 10, is used to define the stress strain curve of the material.

The static yield stress of the material is represented by $\sigma_0$. The elastic limit strain is $\varepsilon_0$. According to von Mises yield criterion, the elastic limit of shear stress is given by $\tau_0=\sigma_0/\sqrt{3}$. The elastic limit of strain components are given by

$$\varepsilon_0=\sigma_0/E \tag{9}$$

$$\gamma_0=\tau_0/G \tag{10}$$

where $E$ and $G$ are the elastic modulus and shear modulus of the material, respectively.

If the stiffened plate enters the plastic deformation stage $\varepsilon>\varepsilon_0$, the elastic-plastic membrane strain energy of the stiffened plate is given as:

$$U_{c\text{-}mp}=\int_0^l\int_0^l\int_0^\delta\left[\sigma_0\varepsilon_x+\sigma_0\varepsilon_y+\tau_0\gamma_{xy}-\frac{1}{2}(\sigma_0\varepsilon_0+\sigma_0\varepsilon_0+\tau_0\gamma_0)\right]dxdydz \tag{11}$$

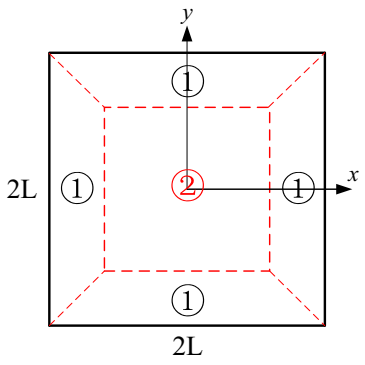


**Fig. 8.** Deformation mode of blast loaded stiffened plate with clamped supports (①, surrounding parts; ②, central part).

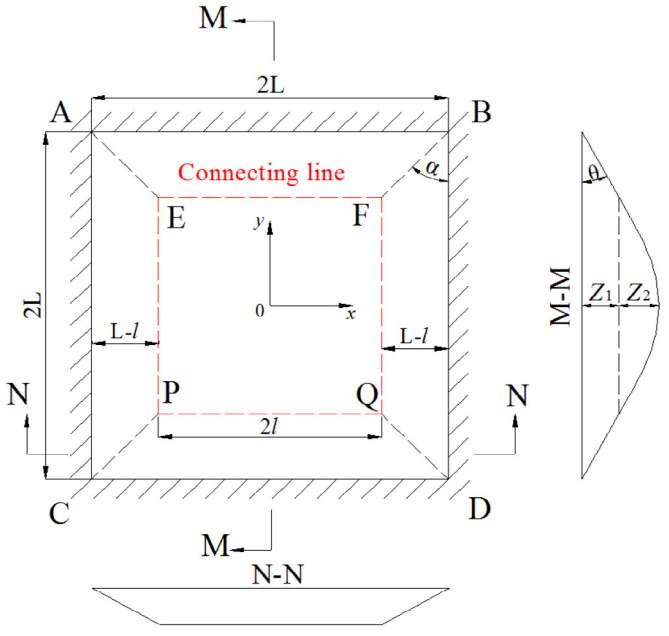


**Fig. 9.** Assumed mode of deformation of clamped square stiffened plates subject to blast loads.

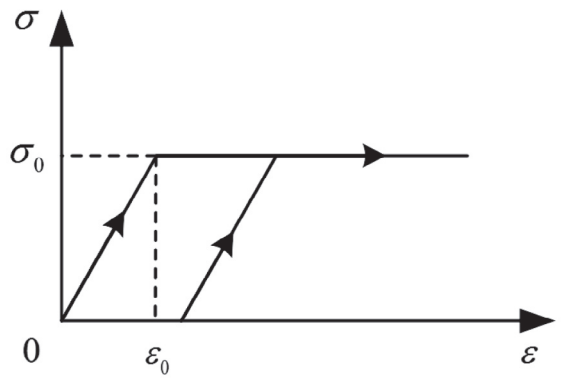


**Fig. 10.** Stress–strain relation of elastic perfectly-plastic materials.

### 3.3. Strain energy of surrounding parts of plate

The shape function given in Eq. (2) is used to represent the global deformation of the surrounding parts of plates, as indicated in Fig. 11. As the surrounding parts of plate are defined as planar stretch zone, the influence of bending effects is neglected.

The elastic strain energy of the plate in surrounding parts is given by:

$$U_{\text{s-me}} = \int_0^{L+l}\int_0^{L-l}\int_0^{\delta}\frac{1}{2}E\varepsilon^2 dxdydz \tag{12}$$

As the rotation angle of yield lines at the clamped edges $\theta$ is very small, it can be considered to be equal to $\tan\theta$ approximately.

$$\theta \approx \tan\theta = \frac{Z_1}{L-l} \tag{13}$$

Therefore, the in-plane strain at any point in surrounding parts of the plate, as indicated in Fig. 12, is given by:

$$\varepsilon = \frac{\left(\sqrt{1+\tan^2\theta}-1\right)(L-l)}{L-l} = \frac{1}{2}\left(\frac{Z_1}{L-l}\right)^2 \tag{14}$$

After the yielding occurs, the plastic strain energy of the plate in surrounding parts is given by:

$$U_{\text{s-mp}} = \int_0^{L+l}\int_0^{L-l}\int_0^{\delta}\left(\sigma_0\varepsilon - \frac{1}{2}\sigma_0\varepsilon_0\right)dxdydz \tag{15}$$

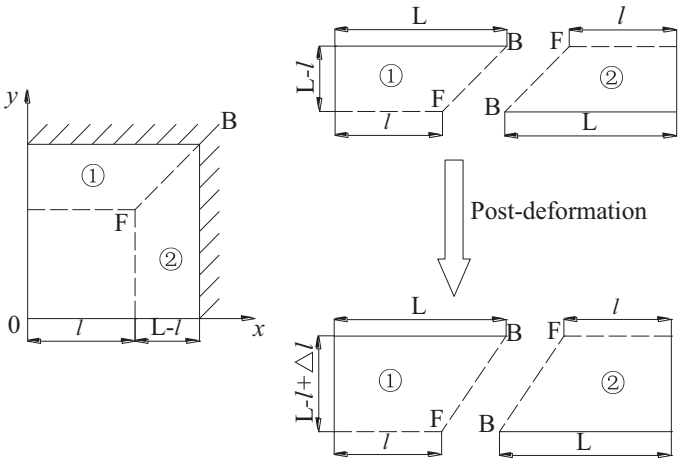


**Fig. 11.** Schematic plot of surrounding parts of deformed square plate.

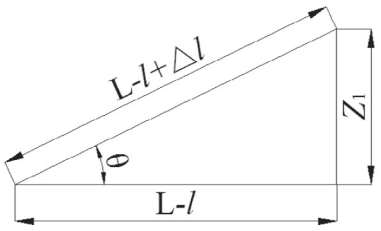


**Fig. 12.** Schematic plot for rotation angle of surrounding part of deformed square plate at clamped edges.

### 3.4. Strain energy of plastic hinges

#### 3.4.1. Rotation angle of plastic hinges

The rotation angle of surrounding part around yield line at clamped edge is represented by $\theta$. The relative rotation angle between central and surrounding part around connecting line is represented by $\theta-\theta_1$. $\theta_1$ is the rotation angle of central part around the connecting line, which is given by:

$$\theta_1 \approx \tan\theta_1 = -\left.\frac{\partial w_2}{\partial x}\right|_{x=l} = \frac{\pi Z_2}{2l}\cos\frac{\pi y}{2l} \tag{16}$$

In general, it is assumed that along the x axis ( $y=0$) or the y axis ( $x=0$), the rotation angle of central part and surrounding part around the connection line between these two parts is considered to be approximately equal, and denoted as $\theta$:

$$\theta \approx \tan\theta = -\left.\frac{\partial w_2}{\partial x}\right|_{\substack{x=l\\y=0}} \tag{17}$$

Substituting Eq. (3) and Eq. (13) into Eq. (17), the ratio between generalized transverse displacements $Z_1$ and $Z_2$ is given by:

$$\frac{Z_1}{Z_2} = \frac{\dot{Z}_1}{\dot{Z}_2} = \frac{\ddot{Z}_1}{\ddot{Z}_2} = \frac{\pi(L-l)}{2l} \tag{18}$$

In order to determine the rotation angle of plastic hinges along the diagonals of the plate, a reference plane perpendicular to the yield line BF through point F is given, and this plane is perpendicular to the x–y plane and intersects with it on the line GH, as shown in Fig. 13. The points G and H are the intersection points of the line GH and boundary of the plate. Provided that $Z_1$ is the displacement of point F, the distance between the point F′ and line GH is considered to be equal to $Z_1$. The relative rotation angle between adjacent surrounding parts around yield line BF is represented by $\theta_2$, which is given by

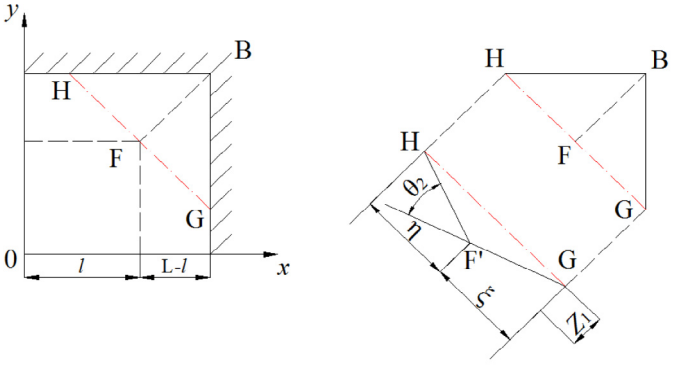


**Fig. 13.** Schematic plot for rotation angle of yield lines in deformed square plate.

$$\theta_2 = Z_1(1/\xi + 1/\eta) \tag{19}$$

$$\xi = l_y \tan\alpha \quad \eta = l_y \cot\alpha \tag{20}$$

where $\alpha$ is the angle between the yield line BF and the boundary BD, and $l_y$ is the length of the yield line BF. Finally, the rotation angle of oblique plastic hinges around the diagonals of plate is given by:

$$\theta_2 = \frac{Z_1}{l}(\cot\alpha + \tan\alpha) \tag{21}$$

For the square stiffened plates, $\alpha = 45°$.

*3.4.2. Strain energy of plastic hinges*

The plastic bending strain energy of the plate per unit width is given by

$$M_p = 2\int_0^{\frac{\delta}{2}} \sigma_0 z dz = \frac{1}{4}\sigma_0 \delta^2 \tag{22}$$

where $\sigma_0$ is the yield strength of material and $\delta$ is the thickness of the plate.

The rotation angle around yield lines at clamped edges is represented by $\theta$. The strain energy of plastic hinge along clamped edges is given by:

$$U_{l1} = \int_0^L \theta M_p dy \tag{23}$$

Similarly, the strain energy of plastic hinges along the connecting lines between central and surrounding part is given by:

$$U_{l2} = \int_0^l (\theta - \theta_1) M_p dy \tag{24}$$

The strain energy of plastic hinges along the diagonals of square plates is given by:

$$U_{l3} = \int_0^{l_y} \theta_2 M_p dx \tag{25}$$

The total energy of plastic hinges in the stiffened plate system is given by:

$$U_l = 2U_{l1} + 2U_{l2} + U_{l3} \tag{26}$$

*3.5. Strain energy of the stiffeners*

In the experimental tests, both ends of stiffeners on the plate are free from boundary constraints. In analytical models, only the flexural strain energy of stiffeners is taken into account while the membrane strain energy is neglected.

Provided that the X position of stiffener is represented by $x_s$, the shape function which represents the global elastic-plastic deformation of the stiffeners is given by:

$$w_s = \begin{cases} Z_1 \cdot \dfrac{L-y}{L-l} & \text{for surrounding part} \\ Z_1 + Z_2 \cos\dfrac{\pi x_s}{2l}\cos\dfrac{\pi y}{2l} & \text{for central part} \end{cases} \tag{27}$$

The strain energy of the stiffener includes the flexural strain energy of the stiffener and the strain energy of the plastic hinges in the stiffener. The flexural strain energy of the stiffener is given by

$$E_{s1} = \frac{1}{2} EI \int_0^l \left( \frac{\partial^2 w_s}{\partial y^2} \right)^2 dy \tag{28}$$

where $I$ is the 2nd moment of area of the stiffener.

The rotation angle of the plastic hinge in the stiffener is given by:

$$\theta_s = -\left.\frac{\partial w_2|_{x=x_s}}{\partial y}\right|_{y=l} = \frac{\pi}{2l} Z_2 \cos\frac{\pi x_s}{2l} \tag{29}$$

Then, the strain energy of the plastic hinge in the stiffener is given by:

$$E_{s2} = M_s(\theta - \theta_s) \tag{30}$$

where $M_s$ is the plastic bending moment at the location of plastic hinge in the stiffener.

Finally, the total strain energy of the stiffeners is given by:

$$U_{st} = E_{s1} + E_{s2} \tag{31}$$

*3.6. Total potential and kinetic energy of the system*

The potential energy loss due to the blast load $p(t)$ is given by:

$$P_E = -\int_0^L \int_0^L p(t) w dx dy \tag{32}$$

The total potential energy of the system (strain energy of all elements of the stiffened plate system and potential energy loss due to blast load) is given by:

$$V = U_{c\text{-}b} + U_{c\text{-}m} + U_{s\text{-}m} + U_l + U_{st} + P_E \tag{33}$$

The kinetic energy of the plate is given by:

$$T_p = \frac{1}{2}\int_0^L \int_0^L \int_0^\delta \rho \dot{w}^2 dx dy dz \tag{34}$$

The kinetic energy of the stiffener is given by

$$T_s = \int_0^L \frac{1}{2} \rho A \dot{w}_s^2 dy \tag{35}$$

where $\rho$ is the density of material, $A$ is the cross-sectional area of the stiffener.

Finally, the total kinetic energy of the stiffened plate system is given by:

$$T = T_p + T_s \tag{36}$$

*3.7. Blast load*

In the theoretical analysis, based on the impulse equivalent principle, the irregular blast loads can be substituted equivalently by a rectangular pressure load which keeps constant within the effective time [20]. In this approach, it is also assumed that the equivalent rectangular pressure load applied uniformly on the stiffened plates. The load–time relation of the equivalent rectangular pressure load is expressed as:

$$p(t) = \begin{cases} P & 0 \le t \le \tau \\ 0 & t \ge \tau \end{cases} \tag{37}$$

*3.8. Lagrange's equation for the blast loaded plates*

The total potential energy and the kinetic energy of the stiffened plate system are related through a non-linear, differential equation by substituting $V$ and $T$ in terms of the generalized displacement $Z_1$ and $Z_2$ into Lagrange's equation:

$$\frac{d}{dt}\left(\frac{\partial T}{\partial \dot{Z}}\right)+\frac{\partial V}{\partial Z}=0 \tag{38}$$

Eq. (38) can be solved numerically using time-stepping numerical integration scheme. In this paper, the fifth-order Runge–Kutta scheme is employed. The solution to the differential equation furnishes the generalized displacement $Z_1$ and $Z_2$ in Eq. (2) and Eq. (3). Then, the dynamic response of the stiffened plate, as indicated in Eq.(1), can be achieved.

## 4. Results and discussion

### 4.1. Numerical simulations of blast loaded plates

In the analytical model that presented in Section 3, the strain rate effect of material was not taken into account and ideal fixed boundary condition was adopted for simplicity. In this part, the influence of these simplified treatments on the predicted results was presented and discussed by means of numerical simulations.

Numerical simulations are performed with the commercial code ANSYS AUTODYN 15.0. In the numerical model, the plates and stiffeners were discretized by the bilinear four-node quadrilateral shell elements with one quadrature point, and the fully coupled Eulerian Lagrangian approaches are employed to simulate the coupling interaction between blast load and stiffened plate. The structural chamber is treated as the rigid boundary of air. The flow-out boundary is applied to the zone where the venting hole located. The fully supported boundary is applied to the clamped part of stiffened plates.

**Table 3**
Mechanical properties of material.

| | |
|---|---|
| Mass density $\rho$ | 7850 kg/m$^3$ |
| Poisson ratio $v$ | 0.28 |
| Young's modulus $E$ | $2.06\times10^{11}$ Pa |
| Yielding stress $A$ | $270\times10^{6}$ Pa |
| Strain hardening modulus $B$ | $275\times10^{6}$ Pa |
| Strain hardening index $n$ | 0.36 |
| Strain rate hardening index $C$ | 0.022 |
| Temperature softening parameter $m$ | 1.03 |

The rotational and translational freedoms of all nodes at the clamped boundary are restrained. The FE model of stiffened plate and fluid is shown schematically in Fig. 14.

The plates and stiffeners are made from Q235 low carbon steel. In numerical simulation, the Johnson–Cook constitutive relation is selected to model the material behavior of the stiffened plates [30].

$$\sigma_d=\left(A+B\varepsilon_p^n\right)\left(1+C\ln\dot{\varepsilon}^*\right)\left(1-T^{*m}\right) \tag{39}$$

where $A, B, C, n$ and $m$ are material parameters. $\varepsilon_p$ is the effective plastic strain, $\dot{\varepsilon}^*=\dot{\varepsilon}_p/\dot{\varepsilon}_0$ is the effective plastic strain rate at a reference strain rate $\dot{\varepsilon}_0=1\,s^{-1}$ and the homologous temperature $T^*=(T-T_r)/(T_m-T_r)$ where $T$ is the material temperature, $T_r$ is the room temperature, and $T_m$ is the melting temperature of material. Mechanical properties of Q235 low carbon steel, summarized in Table 3, are obtained from in-house tests.

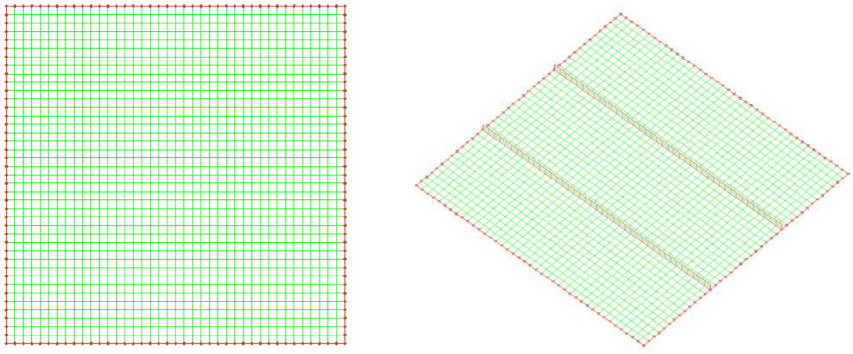

(a) The FE model of stiffened plates

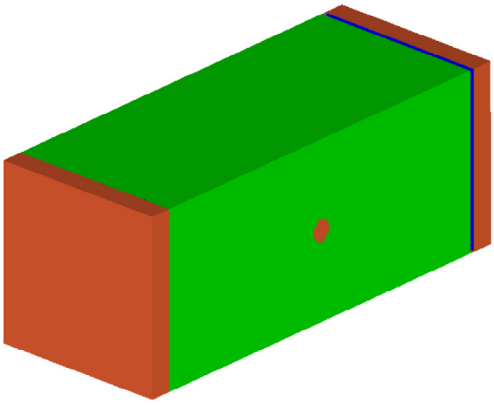

(b) The FE model of air

**Fig. 14.** Full 3-D FE model of stiffened plates and fluid. (a) FE model of stiffened plates. (b) FE model of air.

**Table 4**
Experimental and numerical results of permanent displacements at center of stiffened plates.

| Plate ref. | Experimental results (mm) | Numerical results (mm) | Relative error (%) | Plate ref. | Experimental results (mm) | Numerical results (mm) | Relative error (%) |
|---|---|---|---|---|---|---|---|
| 1 | 35.876 | 35.953 | 0.21 | 6 | 25.919 | 25.046 | –3.37 |
| 2 | 35.374 | 35.449 | 0.21 | 7 | 24.058 | 24.127 | 0.29 |
| 3 | 33.607 | 34.539 | 2.77 | 8 | 22.243 | 21.053 | –5.35 |
| 4 | 24.926 | 26.418 | 5.99 | 9 | 32.408 | 30.596 | –5.59 |
| 5 | 23.502 | 24.451 | 4.04 | 10 | 31.511 | 29.818 | –5.37 |

The displacement and strain histories at the center of plates are selected as output in numerical simulations. The numerical results of permanent displacement of stiffened plates are listed in Table 4. The maximum strain rate of impulsive blast loaded plate is of the order of $\dot{\varepsilon} \approx 10\,s^{-1} - 100\,s^{-1}$ [31]. In dynamic tests, the confined blast load, due to reflection of blast wave, has a long duration and a relatively high peak pressure. As indicated in the numerical results, the maximum strain rate of deflected stiffened panels under internal explosion is about $\dot{\varepsilon} \approx 20 \sim 30\,s^{-1}$. In this range of strain rates, the Johnson–Cook constitutive relation of Q235 low carbon steel predicts a very small change in the flow stress. Another series of numerical simulations not considering material's strain rate are conducted to investigate the influence of strain rate effect on dynamic response of stiffened plates, in which the parameter $C$ in Eq. (39) is set as zero. The results of permanent displacement of stiffened plates in all cases are listed in Table 5. It is found that the strain rate effect of material does not have significant influence on the final deformation of internal blast loaded stiffened plates for the experimental specimens. However, this may not always be the case when highly strain rate sensitive materials are considered or obvious local response and tearing have been observed. It is reasonable to exclude the effect of material's strain rate in the theoretical model for stiffened plates in the experiments considered in the paper.

**Table 5**
The influence of strain rate effect on the permanent displacements of plates in numerical simulations.

| Plate ref. | Numerical results with strain rate effect (mm) | Numerical results without strain rate effect (mm) | Plate ref. | Numerical results with strain rate effect (mm) | Numerical results without strain rate effect (mm) |
|---|---|---|---|---|---|
| 1 | 35.953 | 36.234 | 6 | 25.046 | 25.360 |
| 2 | 35.449 | 35.636 | 7 | 24.127 | 24.437 |
| 3 | 34.539 | 34.620 | 8 | 21.053 | 21.450 |
| 4 | 26.418 | 26.652 | 9 | 30.596 | 30.720 |
| 5 | 24.451 | 24.610 | 10 | 29.818 | 30.023 |

Since the displacement histories of all test plates are similar, the deformation contour plot of stiffened plate in Case 1 is shown in Fig. 15, as an example. It is clearly shown that plate and stiffeners deformed compatibly without evident local deformation. Studies [6,7] have revealed that in-plane displacement at the clamped boundary has significant influence on the large deformation of plate subjected to pulse pressure load. In-plane displacement will result in larger transverse deflection of plates. However, the in-plane displacement at the clamped boundary is strongly related to clamping force, friction interaction and displacement constraints provided by experimental setup (bolts and support plates). If the in-plane clamping force is sufficient or the load intensity is relatively low, the loaded plate experiences relatively small transverse displacement, and the clamped constraint force is almost enough to restrict the in-plane displacement at the clamped boundary. On the other hand, if the clamped boundary is too weak to provide enough clamping force or the load intensity is too high, apparent in-plane displacement

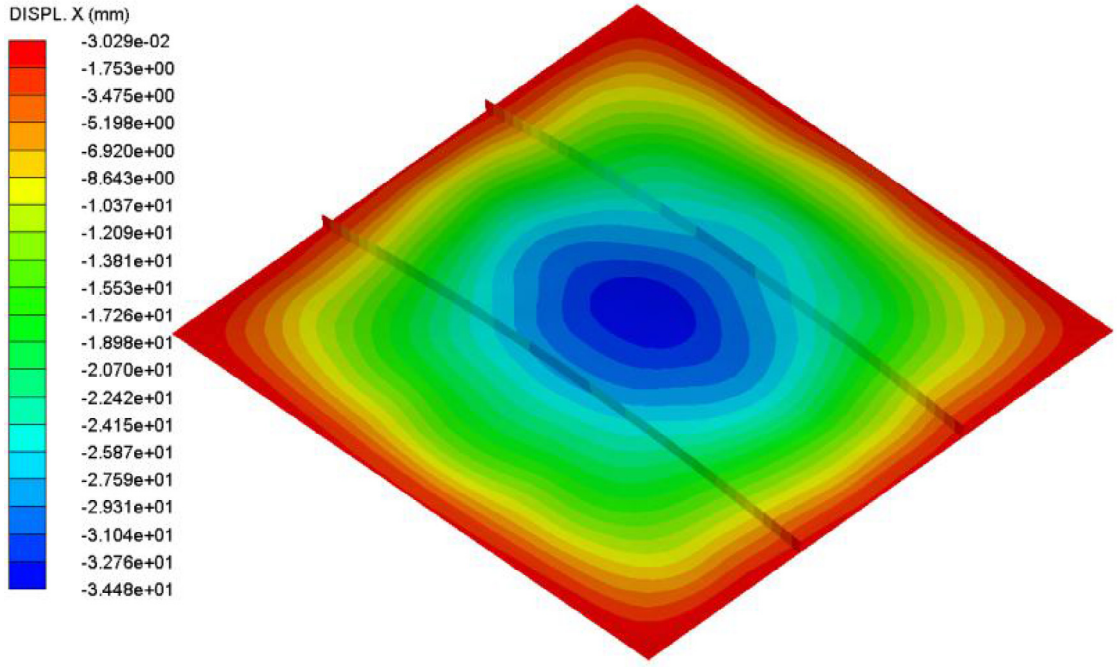


**Fig. 15.** Deformation profile of stiffened plates in Case 1 in numerical simulation.

could be found at the clamped boundary, then it is necessary to take the in-plane displacement into consideration in the theoretical and numerical analysis. As indicated in Table 4, even though the permanent displacements in some cases were underestimated slightly in numerical simulations, good agreement has been achieved between experimental and numerical results with ideal fixed constraints. It is indicated that the in-plane constraints provided by experimental setup is enough in tests. It is reasonable to take the clamped boundary in the experiments as ideal fully fixed condition in the theoretical model.

### 4.2. Results of analytical method

Since the in-plane displacement is small, the strain components originating from $u$ and $v$ could be neglected in the dynamic analysis. The strain components in Eqs. (4)–(6) can be simplified as:

$$\begin{cases} \varepsilon_x = \dfrac{1}{2}\left(\dfrac{\partial w_2}{\partial x}\right)^2 \\ \varepsilon_y = \dfrac{1}{2}\left(\dfrac{\partial w_2}{\partial y}\right)^2 \\ \gamma_{xy} = \dfrac{\partial w_2}{\partial x}\dfrac{\partial w_2}{\partial y} \end{cases} \tag{40}$$

In experimental tests, cylindrical TNT charge was hung in the middle of the chamber to generate blast load for stiffened plates. The blast load in confined space involves the initial shock wave with very short time, several later-reflected pulses and the quasi-static pressure load with a longer duration. The simplified blast loads used in analytical models for test plates are given in Table 6.

The analytical method presented in this paper is employed to predict the elastic-plastic response of test plates in experiments. According to the detailed information described above, the Eq. (38) in Section 2 is solved numerically. Subsequently, the generalized displacements $Z_1$ and $Z_2$ in Eq. (2) and Eq. (3) are determined, and finally the deformation-time history of stiffened plate under confined blast load is obtained by Eq. (1).

Besides, an analytical method presented by Schleyer et al. [4,7], in which the bi-axial behavior of the plate was simulated by a number of strips with finite width that lay in the orthogonal axes of the plate, is used to predict the dynamic response of stiffened plates for comparison.

A classical rigid-plastic analysis is also employed to predict the large plastic deformation of stiffened plates. The empirical equation of rigid-plastic analysis, which is developed to predict the final deformation of plates subjected to explosive loading [8], is given below.

$$\frac{w}{\delta_e} = 0.95\left[\left(1+0.6637\Phi^2\right)^{1/2} - 1\right] \tag{41}$$

where $w$ is the final deformation of the plate, $\delta_e$ is the equivalent plate thickness and $\Phi$ is a non-dimensional number proposed by Nurick and Martin [14], which is defined as follows

**Table 6**
Simplified blast loads of each load case in experiments.

| Load case | Radius of venting hole (mm) | Mass of TNT (g) | Simplified blast load $P$ (kPa) | Load duration $\tau_d$ (ms) |
|---|---|---|---|---|
| 1 | 50 | 55 | 160.0 | 40 |
| 2 | 75 | 110 | 283.0 | 40 |
| 3 | 100 | 200 | 504.3 | 40 |

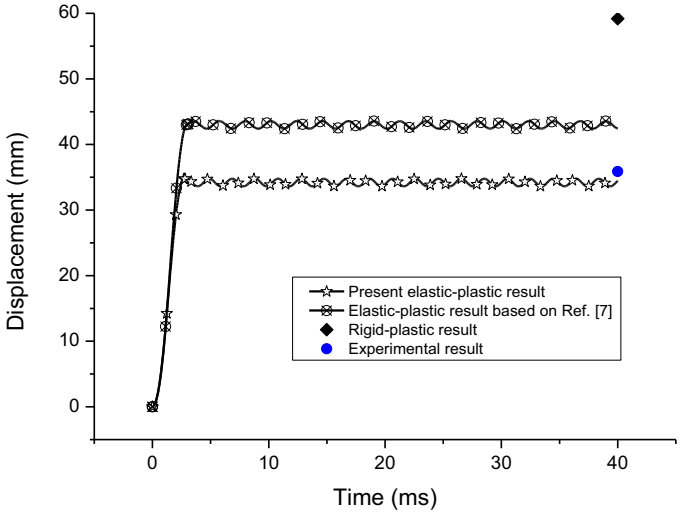


**Fig. 16.** Displacement history at center of plate in Case 1.

$$\Phi = \frac{I_p}{2\delta_e^2\left(4ab\rho\sigma_y\right)^{1/2}} \tag{42}$$

where $I_p$ is the saturated impulse for rectangular pulse load, $a$ and $b$ are half length and width of the plate, respectively, and $\sigma_y$ is the yield stress.

The saturated impulse for simplified rectangular pressure load is defined as

$$I_p = \tau_{sat} P \tag{43}$$

where $P$ is the pressure value of simplified blast load in Eq. (37), $\tau_{sat}$ is the saturated duration of the simplified pressure pulse, which is defined as follows [32]

$$\tau_{sat} = \pi L\sqrt{\frac{\rho}{6\sigma_0}} \tag{44}$$

where $L$ is the length of one-quarter symmetry model, $\rho$ is the density of material, $\sigma_0$ is the static yield stress of material.

In the experiments, all the stiffened plates experienced the similar deformation pattern but with different residual deformation. Theoretical and experimental results are shown in Figs. 16–18 respectively for stiffened plates subjected to different blast loads in cases 1, 7 and 10.

In the present analytical results, the displacement at center of stiffened plates increases rapidly and reaches its maximum value at $t \approx 3$ ms, as shown in Figs. 16–18, in which the blue points represent the experimental results of permanent displacement at center of stiffened plates. The displacement histories of the stiffened plates oscillate after reaching the first peak. After reaching the first peak, the displacement histories get into the rebound phase due to the un-damped elastic oscillation in the theoretical analysis. The permanent displacements of stiffened plate are determined from the average value of the oscillation. As indicated in Figs. 16–18, stiffened plates in different load cases reach the maximum deflection at almost the same time. With the increasing of plate thickness, the displacement of subsequent spring back of deformed stiffened plate increases accordingly, because more elastic energy is stored in thicker plate.

Theoretical and experimental results of the center permanent displacement are given in Table 7 for all stiffened plates. It is noted that the permanent deformation of stiffened plates are severely over-predicted by rigid-plastic model in all cases. The duration of the

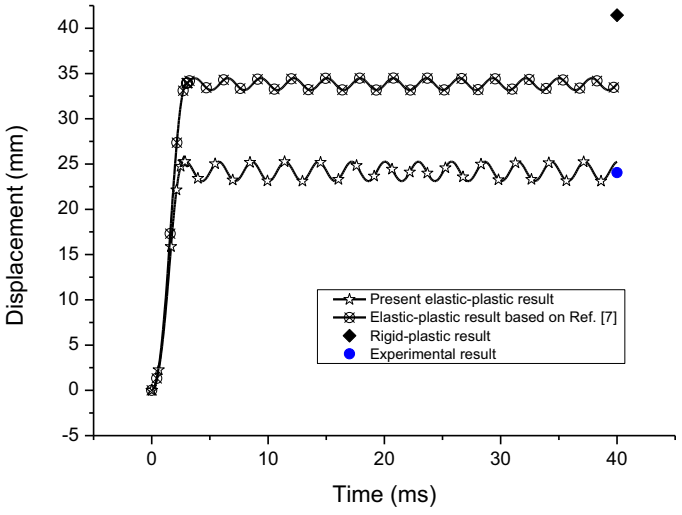


**Fig. 17.** Displacement history at center of plate in Case 7.

confined blast load is not sufficiently short compared with the fundamental elastic period of clamped stiffened plates, which are denoted as $\tau_d$ and $T_f$, respectively. In the paper, the fundamental elastic period of each stiffened plate is obtained through finite element analysis, as listed in Table 8. Studies [6,23] have revealed

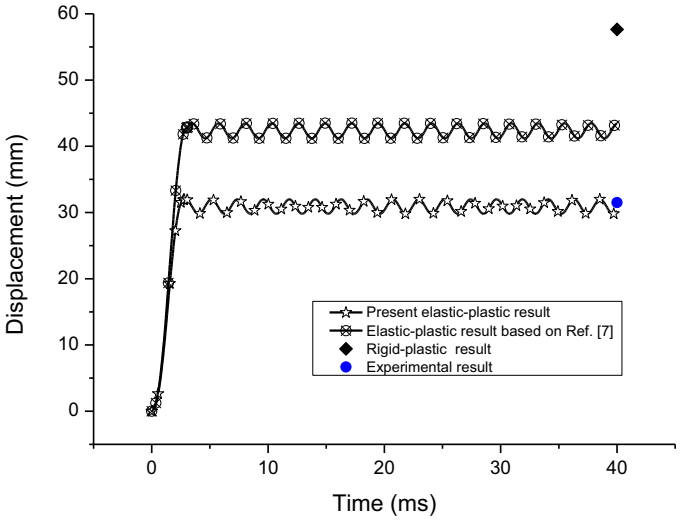


**Fig. 18.** Displacement history at center of plate in Case 10.

**Table 7**
Permanent displacement at center of plate predicted by different methods.

| Plate ref. | Experimental results (mm) | Rigid-plastic results (mm) | Elastic-plastic Results based on Ref. [7] (mm) | Present elastic-plastic results (mm) | Relative error (%) |
|---|---|---|---|---|---|
| 1 | 35. 876 | 59.180 | 42.983 | 34.200 | –4.67 |
| 2 | 35.374 | 58.447 | 42.381 | 33.797 | –4.46 |
| 3 | 33.607 | 56.901 | 41.878 | 33.421 | –0.55 |
| 4 | 24.926 | 39.000 | 31.543 | 23.979 | –3.80 |
| 5 | 23.052 | 37.533 | 31.502 | 23.465 | +1.79 |
| 6 | 25.919 | 42.702 | 33.929 | 24.556 | –5.26 |
| 7 | 24.058 | 41.448 | 33.826 | 24.187 | +0.54 |
| 8 | 22.243 | 40.252 | 32.127 | 22.770 | +2.37 |
| 9 | 32.408 | 58.719 | 42.850 | 31.164 | –3.84 |
| 10 | 31.511 | 57.637 | 42.337 | 30.903 | –1.93 |

**Table 8**
Fundamental elastic period and ratio of blast load duration to fundamental elastic period for each stiffened plate.

| Plate ref. | Load duration $\tau_d$ (ms) | Fundamental elastic period $T_f$ (ms) | Ratio of load duration to fundamental elastic period $\tau_d/T_f$ |
|---|---|---|---|
| 1 | 40 | 20.9 | 1.914 |
| 2 | 40 | 17.4 | 2.299 |
| 3 | 40 | 15.8 | 2.532 |
| 4 | 40 | 12.9 | 3.101 |
| 5 | 40 | 11.4 | 3.509 |
| 6 | 40 | 10.9 | 3.670 |
| 7 | 40 | 10.5 | 3.810 |
| 8 | 40 | 8.3 | 4.819 |
| 9 | 40 | 10.7 | 3.738 |
| 10 | 40 | 9.4 | 4.255 |

that elastic effects could be neglected when the load pulse duration is sufficiently short with respect to the fundamental elastic period.

As indicated in Table 8, the ratio $\tau_d/T_f$ for confined blast load is larger than 1 and do not conform to the prerequisite of the rigid-plastic model. Therefore, the rigid-plastic solution overestimates the permanent displacement of plates. However, the elastic-plastic methods give more accurate results in all cases, as shown in Figs. 16–18. From experimental results, it is noted that the permanent displacement of stiffened plate is more sensitive to thickness of plate rather than to size of the stiffeners attached to plate. It is evident that the effect of membrane force plays an important role in dynamic process when relatively large deformation occurs in blast loaded stiffened plate. Compared to the experimental data, the results of present analytical method, which takes the effect of yield lines and deformation pattern of stiffened plates into consideration, achieve good agreement with experimental results, as listed in Table 7. The relative errors are less than 6% in all cases. Besides, the permanent displacements obtained by present analytical method and the elastic-plastic models in Schleyer et al. [7] are compared, which revealed that the accuracy of the theoretical approach is related to the shape function used to represent the deformed shape of the stiffened plates. The results of present analytical method considering the influence of yield line pattern agree better with experimental results than those of rigid-plastic method [8] and analytical method proposed by Schleyer et al. [7]. The exact deformed shape in analytical models would result in more accurate prediction of dynamic elastic-plastic response of square stiffened plates subjected to confined blast loads.

## 5. Conclusions

This paper aims to investigate the behavior of square stiffened plates under confined blast load through analytical and experimental methods. A device for experiments of plates under confined blast load was designed, and experimental tests of ten specimens were conducted. From experimental observations and measurements, it is revealed that the final deformation of stiffened plates is more sensitive to thickness of plate than size of stiffeners attached to plate, which means that the non-linear membrane effect plays an important role in the dynamic process.

The dynamic response of stiffened plates under confined blast load with a relatively long duration is greatly different from that subjected to impulsive load of open space explosion. When the ratio of the blast load duration to fundamental elastic period is not sufficiently small, the elastic effect has remarkable influences on the dynamic response of stiffened plates, and the classical rigid-plastic method would overestimate the permanent displacement of stiffened plates. The rotation of plastic hinges consumed energy

from blast events, and thus the total deflection of plate is usually smaller when compared to conditions that the effect of plastic hinges was not considered. Furthermore, yield lines change the deformed shape of plates. Correct description of deformed shape could lead to more accurate modeling of the plates subjected to blast load. The analytical method presented in this paper shows a proper deformation pattern of blast loaded stiffened plates.

From the comparison between experimental and theoretical results, the present theoretical method gives good prediction of the data from experiments, which validates that the analytical method proposed in this paper can provide adequate predictions of the behavior of dynamic large deformation of confined blast loaded plates.

## Acknowledgements

The authors acknowledge the support of National Defense Fundamental Research Project (B1420133057), National Natural Science Foundation of China (51409202 and 11502180) and the Fundamental Research Funds for the Central Universities (2015-yb-005). The authors wish to express gratitude to Dr. Hou Hai-liang for his valuable help during experimental tests.

## References

[1] Nurick GN, Olson MD, Fagnan JR, Levin A. Deformation and tearing of blast-loaded stiffened square plates. Int J Impact Eng 1995;16(2):273–91.
[2] Chung Kim Yuen S, Nurick GN. Experimental and numerical studies on the response of quadrangular stiffened plates. Part I: subjected to uniform blast load. Int J Impact Eng 2005;31(1):55–83.
[3] Langdon GS, Yuen SCK, Nurick GN. Experimental and numerical studies on the response of quadrangular stiffened plates. Part II: localised blast loading. Int J Impact Eng 2005;31(1):85–111.
[4] Neuberger A, Peles S, Rittel D. Springback of circular clamped armor steel plates subjected to spherical air-blast loading. Int J Impact Eng 2009;36(1):53–60.
[5] Kong X, Wu W, Li J, Chen P, Liu F. Experimental and numerical investigation on a multi-layer protective structure under the synergistic effect of blast and fragment loadings. Int J Impact Eng 2014;65:146–62.
[6] Schleyer GK, Hsu SS. A modelling scheme for predicting the response of elastic–plastic structures to pulse pressure loading. Int J Impact Eng 2000;24(8):759–77.
[7] Schleyer GK, Hsu SS, White MD, Birch RS. Pulse pressure loading of clamped mild steel plates. Int J Impact Eng 2003;28(2):223–47.
[8] Jones N. Structural impact. Cambridge: Cambridge University Press; 1989 (Paperback edition 1997).
[9] Jones N. Impact loading of ductile rectangular plates. Thin Wall Struct 2012;50(1):68–75.
[10] Jones N. Dynamic inelastic response of strain rate sensitive ductile plates due to large impact, dynamic pressure and explosive loadings. Int J Impact Eng 2014;74:3–15.
[11] Jiang J, Olson MD. Rigid-plastic analysis of underwater blast loaded stiffened plates. Int J Mech Sci 1995;37(8):843–59.
[12] Yankelevsky DZ. Elasto-plastic blast response of rectangular plates. Int J Impact Eng 1985;3(2):107–19.
[13] Imam BM, Collins J. Assessment of flat deck metallic plates-yield line and membrane analyses. J Construct Steel Res 2013;82:131–41.
[14] Nurick GN, Martin JB. Deformation of thin plates subjected to impulsive loading – a review, part II: experimental studies. Int J Impact Eng 1989;8:171–86.
[15] Nurick GN, Martin JB. Deformation of thin plates subjected to impulsive loading – a review, part I: theoretical considerations. Int J Impact Eng 1989;8(2):159–70.
[16] Baker WE. Approximate techniques for plastic deformation of structures under impulsive loading. Shock Vib Dig 1975;7:107–17.
[17] Biggs JM. Introduction to structural dynamics. New York: McGraw-Hill College; 1964. p. 188–95.
[18] Fallah AS, Louca LA. Pressure–impulse diagrams for elastic-plastic-hardening and softening single-degree-of-freedom models subjected to blast loading. Int J Impact Eng 2007;34(4):823–42.
[19] Izadifard R, Maheri M. Application of displacement-based design method to assess the level of structural damage due to blast loads. J Mech Sci Technol 2010;24(3):649–55.
[20] Peng Y, Yang P. Dynamic plastic response of clamped stiffened plates with large deflection. J Mar Sci Appl 2008;7(2):82–90.
[21] Rigby SE, Tyas A, Bennett T. Single-degree-of-freedom response of finite targets subjected to blast loading – the influence of clearing. Eng Struct 2012;45:396–404.
[22] Rigby SE, Tyas A, Bennett T. Elastic–plastic response of plates subjected to cleared blast loads. Int J Impact Eng 2014;66:37–47.
[23] Symonds PS, Frye CWG. On the relation between rigid-plastic and elastic-plastic predictions of response to pulse loading. Int J Impact Eng 1988;7(2):139–49.
[24] Schleyer G, Mihsein M. Development of mathematical models for dynamic analysis of structures. Conference proceedings on structural design against accidental loading-as part of the offshore safety case, London. 1992, p. 3.2.1–11.
[25] Schleyer GK, Campbell D. Development of simplified analytical methods for predicting the response of offshore structures to blast and fire loading. Mar Struct 1996;9(10):949–70.
[26] Schleyer GK, Hsu SS, White MD. Blast loading of stiffened plates: experimental, analytical and numerical investigations, ASME/JSME joint pressure vessels and piping conference. San Diego, CA, USA: ASME; 1998. PVP-Vol. 361. p. 237–55.
[27] Langdon GS, Schleyer GK. Inelastic deformation and failure of clamped aluminium plates under pulse pressure loading. Int J Impact Eng 2003;28(10):1107–27.
[28] Langdon GS, Schleyer GK. Inelastic deformation and failure of profiled stainless steel blast wall panels. Part II: analytical modelling considerations. Int J Impact Eng 2005;31(4):371–99.
[29] Turvey GJ, Salehi M. Elasto-plastic large deflection response of pressure loaded circular plates stiffened by a single diametral stiffener. Thin Wall Struct 2008;46(7–9):991–1002.
[30] Johnson G, Cook W. A constitutive model and data for metals subjected to large strain, high strain rates and high temperature. Proceedings of the 7th international symposium on ballistics, The Hague, The Netherlands. 1983, p. 541–8.
[31] Zhu X. The experimental study of dynamic yielding stress on “921A” steel. J Naval Univ Eng 1991;2(1):43–8.
[32] Zhao Y-P. Saturated duration of rectangular pressure pulse applied to rectangular plates with finite-deflections. Mech Res Commun 1997;24(6):659–66.